ROYAL SOCIETY OF CHEMISTRY

Check for updates

# Merging polyacenes and cationic helicenes: from weak to intense chiroptical properties in the far red region†

Romain Duwald,[a] Johann Bosson, [a] Simon Pascal, [a] Stéphane Grass,[a] Francesco Zinna, [ab] Céline Besnard, [c] Lorenzo Di Bari, [b] Denis Jacquemin [*d] and Jérôme Lacour [*a]

A series of helical tetracenes and pentacenes was synthesized from cationic [6] and [4]helicene precursors. These colorful acenes fluoresce in the far red region. While [4]helicene-based pentacenes exhibit chiroptical properties mainly in the UV region, [6]helicene-derived tetracenes show enhanced ECD in the visible range, in addition to clear CPL responses. This difference is rationalized using first principles.

Polyacenes, linearly fused polycyclic aromatic hydrocarbons or PAHs, are strongly studied for their electronic properties.[1] Thanks to their narrow HOMO–LUMO gap, these compounds are efficient charge transport materials,[2] with potential applications in semi-conductors, thin-film and light emitting devices.[1c,e,3] Their heterocyclic analogs, and more specifically aza heteroacenes,[1e,f,4] show improved resistance to oxidative degradation[5] while maintaining their exceptional electronic behavior. Alternatively, helicenes, that are *ortho* fused polyaromatic systems and inherently chiral molecules, can be used.[6] These entities are involved in various applications spanning from physical chemistry to biochemistry and catalysis.[7] Helicenes generally possess optical properties in the blue part of the visible light spectrum, although both push–pull systems[8] and cationic helicenes[9] see their optical properties shifted toward the red domain. In addition, the chiroptical properties of helicenes have been intensively scrutinized,[10] including their ability to emit circularly polarized light.[10,11] Herein, the privileged polyacene and helicene motifs are merged into single frameworks to provide polyaza helical acenes 1–6 (Fig. 1).[12] These

derivatives, prepared by late-stage introduction of *N*-phenylquinolone motifs at internal or terminal extremities of cationic [4] or [6]helicenes 7 and 8 (Scheme 1, 3–5 steps),[13] are colorful dyes emitting in the far red region.[14] Tetracenes 4–6 exhibit strong electronic circular dichroism (ECD) and circularly polarized luminescence (CPL) properties in the whole visible domain while pentacenes 1–3 mainly display ECD in the UV spectral range, an outcome rationalized using *ab initio* calculations.

To prepare polyaza acenes 1–6, recent developments on the late-stage functionalization of cationic [4] or [6]helicenes were used.[9a,15] With 7 as substrate, three regioselective routes to pentacenes 1–3 were developed (Scheme 1, top). Under mild conditions,[9a] ketone K1 was obtained in three steps *via* a selective formylation of 7 at position 6 or 8 (46% overall yield). In strongly acidic conditions, benzoylations of 7 occurred at positions 2 and/or 12 instead.[15] With an excess of 2-bromobenzoic acid in Eaton's reagent (MsOH, $P_2O_5$),[16] ketone K2 was obtained in 93% yield. From K2, in even more
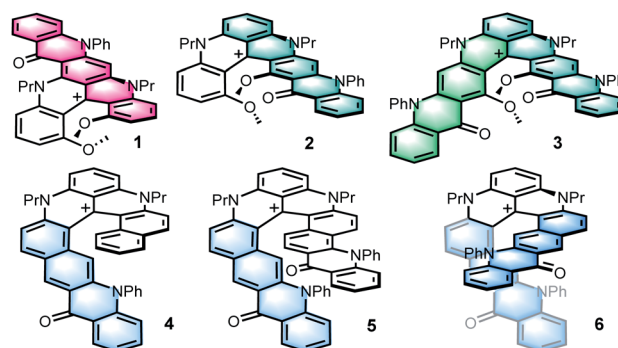
*aDepartment of Organic Chemistry, University of Geneva, Quai Ernest Ansermet 30, 1211 Geneva 4, Switzerland. E-mail: jerome.lacour@unige.ch*

*bDipartimento di Chimica e Chimica Industriale, Università di Pisa, Via Moruzzi 13, 56124 Pisa, Italy*

*cLaboratoire de Cristallographie, University of Geneva, Quai Ernest Ansermet 24, 1211 Geneva 4, Switzerland*

*dCEISAM, UMR CNRS 6230, Université de Nantes, 2 rue de la Houssinière, 44322 Nantes, France. E-mail: Denis.Jacquemin@univ-nantes.fr*

Fig. 1 Helical pentacenes 1–3 and tetracenes 4–6. *M* enantiomers shown.
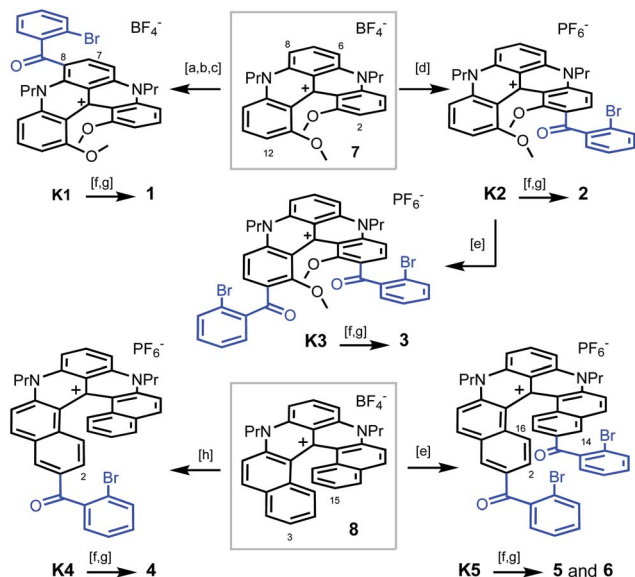
**Scheme 1** Synthesis of pentacenes **1**–**3** from [4]helicene **7** (top) and tetracenes **4**–**6** from [6]helicene **8** (bottom): [a] $POCl_3$, DMF, 90 °C; [b] [(2-bromophenyl)magnesium bromide·LiCl],[19] $CH_2Cl_2$, 0 °C; [c] PCC, $CH_2Cl_2$, 40 °C; [d] 2-bromobenzoic acid, Eaton's reagent, 60 °C; [e] 2-bromobenzoic acid, TfOH, $P_2O_5$, 50 or 80 °C; [f] $PhNH_2$, Pd(OAc)$_2$, *rac*-BINAP, $Cs_2CO_3$, DMF, 90 or 100 °C; [g] CuI, 2,2′-bipyridine, DMF or NMP, air, 90 or 130 °C; [h] 2-bromobenzoic acid, PPA, 100 °C. **1** is isolated as a $BF_4^-$ salt, **2**–**6** as $PF_6^-$ salts.

acidic conditions (TfOH, $P_2O_5$), a second regioselective benzoylation was possible to afford **K3** (40%). Then, with bromide **K1**–**K3** in hand, final aza ring closures were achieved by sequences of Pd-catalyzed Buchwald–Hartwig reactions (introduction of NPh groups in place the bromine atoms),[17] and Cu-catalyzed oxidative (air) C–N bond formations closing the acridone ring and thus completing the acene extension.[18] Starting from **7**, pentacenes **1**, **2** and **3** were thus afforded in 24%, 41% and 13% yields in 5-, 3- and 4-step procedures respectively.

With [6]helicene **8** as substrate, tetracenes **4**–**6** were prepared using similar procedures and conditions to that above described. They are summarized at the bottom of Scheme 1.[15] Depending on the acidic medium used,[20] intermediates **K4** and **K5** were prepared in single steps. They were then engaged directly in the Buchwald–Hartwig/oxidative ring closure sequence. Using **K4**, after the Pd-catalyzed Br → NPh exchange, the aza ring closure occurred under oxidative coupling conditions at position **2** preferentially to yield **4** (combined yield 15% from **8**). From **K5**, two regioisomers were isolated after the second oxidative acridone ring closure, $C_1$-symmetric **5** (C-2 and C-14 reactivity) along with $C_2$-symmetric regioisomer **6** (C-2 and C-16 reactivity). Products **5** and **6** were isolated in 10% and 9% combined yields from **8**, respectively. In this series, and of importance to explain both the lower yields and some of the later properties, let us underline that the phenylaniline substituents are primarily introduced in the sterically encumbered interior and not on the outer rim of the helicene as in compounds **1** to **3**.

Helical polyacenes **1**–**6** were bench and moisture stable and the $BF_4^-$ or $PF_6^-$ salts could be characterized as any other organic material (see the ESI†). Solid-state structures of acenes **2**, **4**, and **6** were also studied by X-ray diffraction analyses (Fig. 2). Key structural features like the dihedral angles and helical pitches are provided in Table 1 and in the ESI.† Unsurprisingly, the presence of aromatic phenyl groups on the inner rim of the helicenes (inside the fjord region) strongly increases the helicity from **2** to **4** and then **6**. Nevertheless, there is enough space inside the groove to accommodate a quasi-perpendicular arrangement of the extra Ph ring(s). The angles between the mean planes of the pyridinone and phenyl motifs are 75° for **4**, and 79° and 86° for Ph groups of **6** respectively. With this amplification and based on precedents,[21] larger chiroptical responses were foreseen for the later derivatives. The helical pitch determined by DFT (Density Functional Theory) in solution are very similar (*vide infra*).

As mentioned, helicenes **1**–**6** are colorful dyes and efficient fluorophores. Their optical properties were investigated in acetonitrile (*ca.* $10^{-5}$ M, see the ESI†). In the [4]helicene series (**1**–**3**, Fig. 3 top), strong modifications of the absorption spectra were observed in the visible range as compared to parent **7** that presents a lowest energy transition at 616 nm with a shoulder at higher energy.[9a] Pentacene **1** exhibits a lowest energy transition peaking at 576 nm. This blue-shift, compared to **7**, is inherent to the electron-withdrawing ketone functional group at the C-6/C-8 position. Conversely, pentacene **2** is red-shifted compared to **1** with a $\lambda_{max}$ of absorption at 620 nm, and three maxima of similar intensities appear in the 500–600 nm range. Further bathochromic shift is observed for the bis pentacene **3** that presents a broad absorption between 500 and 700 nm with a $\lambda_{max}$ at 572 nm. Overall, relative to parent **7**, the lowest energy transitions of **2** and **3** are hardly shifted. The same trend is observed in fluorescence with blue and red-shifts of the emissions for **1**, and **2**–**3** compared to parent [4]helicene **7**. The fluorescence quantum yield of **1**–**3** is similar to that of **7** ($\phi$ = 0.15, 0.09 and 0.04 *vs.* 0.13 for **1**, **2**, **3** and **7** respectively). In contrast, the elongation of the naphthalene part of [6]helicene **8** has only a marginal influence on the optical properties (Fig. 3, bottom).[9b] In fact, for **4** and **6**, the lowest energy transitions are centered around 614–616 nm with a shoulder at higher energies and present a moderate hypochromic shift compared to parent
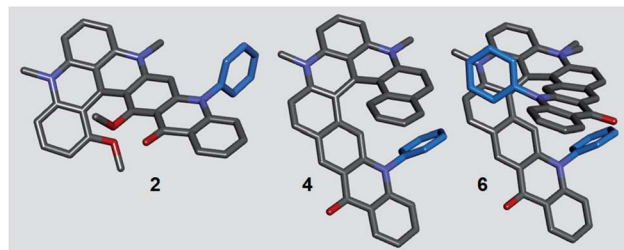
**Fig. 2** Stick view of the crystal structures of **2**, **4** and **6**. For clarity reasons, hydrogen atoms, propyl side chains and counterions are omitted or truncated. *N*-phenyl groups are drawn in blue. For **6**, due to disorder, two side chain residues appear on one *N*-atom, see ESI.†

**Table 1** Key geometrical parameters for **2**, **4** and **6**[a]

| Helical acene | Dihedral angle (°) | Helical pitch (Å) |
| --- | --- | --- |
| **2** | 46.8 | 2.66 |
| **4** | 44.7 | 3.09 |
| **6** | 50.8 | 3.28 |

[a] Dihedral angles defining the fjord region are common descriptors for [4] and [6]helicene scaffolds (see ESI). The helical pitch is the distance between the first two overlapping atoms of the helicene.
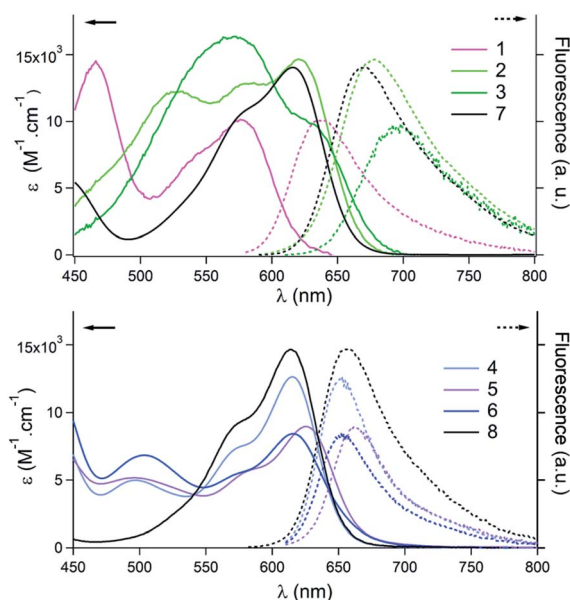


**Fig. 3** Absorption (plain lines) and emission (dashed lines) spectra in acetonitrile. Top: pentacenes **1–3** and comparison to [4]helicene **7**. Bottom: tetracenes **4–6** and comparison to [6]helicene **8**.
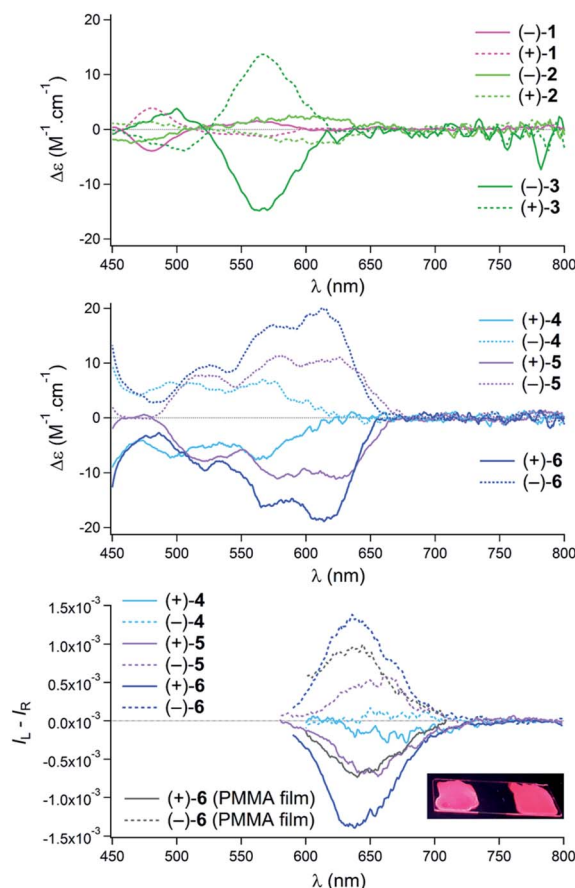


**Fig. 4** Top: ECD spectra in acetonitrile for 1 eluted (plain lines) and 2nd eluted (dashed lines) enantiomers of pentacenes **1–3**. Middle: ECD spectra in acetonitrile for 1 eluted (plain lines) and 2nd eluted (dashed lines) enantiomers of tetracenes **4–6**. Bottom: CPL of **4–6** in acetonitrile and **6** in PMMA films for 1 eluted (plain lines) and 2nd eluted (dashed lines) enantiomers; insert: picture of the films under UV light irradiation.

**8**. The absorption of **5** is very slightly red-shifted to 625 nm. In terms of fluorescence, the emissions are centered at 653, and 656 nm for **4** and **6**, and at 658 nm for parent **8**. Again a small bathochromic shift is observed for **5** that fluoresces at 663 nm. The fluorescence quantum yields in acetonitrile (0.29, 0.25 and 0.21 for **4**, **5** and **6**) are similar to that of **8** ($\phi = 0.31$).[9b]

Regarding the chiroptical properties,[22] striking differences are noted, this time, in favor of [6]helicene-derived **4–6** over pentacenes **1–3**. For all compounds, single enantiomers were obtained by mean of chiral stationary phase (CSP) HPLC (see Fig. S1–S12†). Noticeably, the ECD spectra of pentacenes **1** and **2** exhibit only very weak Cotton effects in the visible range (Fig. 4, top). Bis pentacene **3** presented a more intense response but only for the absorption band in the 520–600 nm region ($\Delta\varepsilon = +$ or $-15$ $M^{-1}$ $cm^{-1}$ at 574 nm) and not for the lowest-energy peak.[23] For derivatives **4–6**, Cotton effects were observed for the lowest energy transitions around 620 nm (Fig. 4, middle). Interestingly, an increase is noted from mono **4** to "distorted" **5** and finally to **6** ($\Delta\varepsilon = +$ or $-7$, 10 and 18 $M^{-1}$ $cm^{-1}$ for **4**, **5** and **6**, respectively).[23] The circularly polarized luminescence (CPL) of helicenes **1–6** was also recorded in acetonitrile solutions.[9b,c,11,24]

For derivatives **1–3**, the $g_{lum}$ values were below the detection limit and are not displayed. In sharp contrast, helicenes **4–6** were effective CPL emitters (Fig. 4, bottom). While mono tetracene **4** presented at the fluorescence wavelength only an anisotropy factor $g_{lum}$ of $1 \times 10^{-4}$, non-symmetrical **5** exhibited a $g_{lum}$ value of $6 \times 10^{-4}$ at 650 nm. Finally, bis tetracene **6** was characterized by a $g_{lum}$ value of $1.4 \times 10^{-3}$ at 640 nm. This trend of the $g_{lum}$ values of **4–6** is similar to that of the $g_{abs}$ values for the most red-shifted Cotton effects. This is an indication that major geometry variations do not occur between ground and emitting excited states; first principles calculations will confirm this observation (*vide infra*).[25] With derivative **6**, CPL was also measured in the solid state. For that purpose, samples were dispersed at a 0.5% weight level in methyl polymethylmethacrylate (PMMA) and the mixture was deposed on a quartz plate affording a $g_{lum}$ value of $8 \times 10^{-4}$ at 640 nm.[26] In view of the marked contrast between the (chir)optical properties of pentacenes **1–3** on one side and **4–6** on the other, care was taken to gain a larger understanding of the dichotomic behavior through first principles analysis.

The details of the applied theoretical protocol are given in the ESI.† The helical pitches determined by DFT in solution are 2.69, 2.61, 2.59, 3.18, 3.15, and 3.20 Å for **1**, **2**, **3**, **4**, **5**, and **6**, respectively. In the instance of compounds **2**, **4** and **6**, featuring experimental XRD values (Table 1), an excellent agreement is noticed, suggesting modest changes in solution. Clearly, helical pitches are significantly larger in the tetracene **4–6** series than in pentacenes **1–3**. In the lowest excited-states, pitches remain very similar: 2.71, 2.63, 2.62, 3.27, 3.09, and 3.34 Å for **1**, **2**, **3**, **4**, **5**, and **6**, respectively, confirming the rigidity of the systems, which is consistent with the rather moderate Stokes shift noted experimentally (Fig. 3).

The vertical transition wavelengths determined with TD (Time-Dependent)-DFT are 459, 499, 503, 507, 512, 507, 491, and 504 nm for **1**, **2**, **3**, **4**, **5**, **6**, **7**, and **8** respectively. These values are obviously blue-shifted compared to the measurements (Fig. 3), which is explainable by the nature of the considered systems and the neglect of vibronic couplings (see the ESI† for discussion, and calculations with higher levels of theory). Nevertheless, the ranking of the TD-DFT and experimental values perfectly agree, with almost no shift in the tetracene series but for a very small red-shift of **5**, and more sizeable effects in the pentacene series with a large blue-shift of **1** as compared to the other members of the series. In Fig. 5, we show density difference plots corresponding to the lowest excited state ($S_1$) for four selected dyes (see the ESI† for other compounds). One finds the typical pattern for such derivative,[9b,c] with alternating lobes of density gain and depletion, the central carbon atom (formally positively charged) acting has a strong acceptor (in red) and the "top" phenyl ring as an electron donor (mostly in blue). In **1**, the pattern of the state is globally preserved (with limited delocalization on the added moiety), but the presence of the carbonyl group renders the donating character of the top phenyl weaker, hence explaining the blue-shift. Nevertheless, one notes overall that the delocalization of the excited state over the added phenyl rings is very limited in all cases, hence the nature of this lowest excited state is mostly preserved in the full series of compounds.

In Table S5 in the ESI,† we report the computed rotatory strengths ($R$) for the five lowest singlet states. For the lowest transition, we note rather small responses (<40 cgs, *ca.* <10 $M^{-1}$ $cm^{-1}$ in the $\Delta\varepsilon$ scale) in the pentacene series **1–3**, but significantly higher responses (up to 218 cgs or *ca.* 38 $M^{-1}$ $cm^{-1}$ for **6**) in the tetracene series **4–6**, which is clearly in line with the experimental data (Fig. 4, top and middle). Theory also restores the outcome that the response is maximal for **5** and **6** and rather negligible for **1** and **2**. As seen above, the electronic nature of the $S_1$ state is globally preserved within all compounds, so that we qualitatively relate the larger ECD response in the tetracene series to their higher helicity, as illustrated by the pitch values (*vide supra*). For the higher-lying transitions, one notices in Table S5† that $R$ values are very diverse in both series, *e.g.*, for $S_2$, TD-DFT predicts $|R|$ of 97 cgs for **1**, 176 cgs for **3**, 48 cgs for **4**, and 282 cgs for **6**. This is consistent with the rather large responses of **3** and **6** at shorter wavelength as compared to **1** and **4** (Fig. 3). This variation as compared to $S_1$ can be explained by the different natures of the $S_2$ excited states that, as can be seen in Fig. S26 in the ESI,† now involve much more importantly the added acene rings as compared to **7** and **8**. Thus, at higher energies, the helical pitch is not a sufficient parameter to understand the experimental responses.

## Conclusions

Through late-stage functionalizations of cationic [6] or [4]helicenes, series of helical tetracenes and pentacenes were prepared. Due to a larger helical pitch (*ca.* 3.2 Å *vs.* 2.6–2.7 Å) and as demonstrated through first principles analyses, only the class of tetracene derivatives exhibit strong ECD and CPL properties in the far red domain, including in the solid state. Based on these enhanced properties, a wealth of developments can be considered.[26b,d,f]

## Conflicts of interest

Authors declares no conflicts of interest.

## Acknowledgements
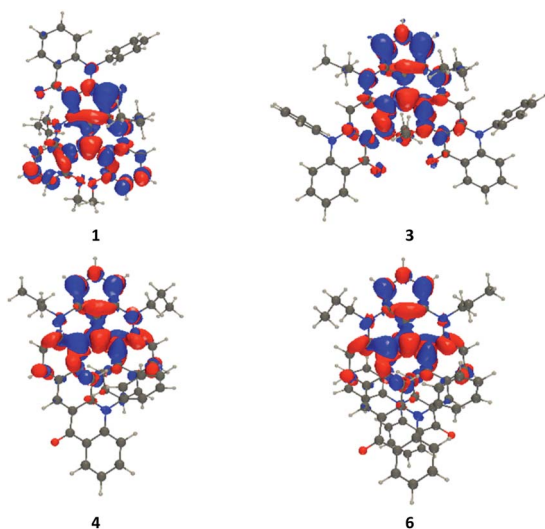
**Fig. 5** Density difference plots for the lowest transition in selected compounds. Blue and red regions indicate decrease and increase of electron density upon electronic excitation, respectively (contour threshold: 0.001 au).

## Notes and references

1 (*a*) J. E. Anthony, *Chem. Rev.*, 2006, **106**, 5028–5048; (*b*) G. J. Richards, J. P. Hill, T. Mori and K. Ariga, *Org. Biomol.*

*Chem.*, 2011, **9**, 5005–5017; (*c*) Q. Miao, *Synlett*, 2012, **2012**, 326–336; (*d*) H. F. Bettinger and C. Toenshoff, *Chem. Rec.*, 2015, **15**, 364–369; (*e*) J. Li and Q. Zhang, *ACS Appl. Mater. Interfaces*, 2015, **7**, 28049–28062; (*f*) U. H. F. Bunz, *Acc. Chem. Res.*, 2015, **48**, 1676–1686.

2 F. Paulus, J. U. Engelhart, P. E. Hopkinson, C. Schimpf, A. Leineweber, H. Sirringhaus, Y. Vaynzof and U. H. F. Bunz, *J. Mater. Chem. C*, 2016, **4**, 1194–1200.

3 D.-K. Kim and J.-H. Choi, *Opt. Mater.*, 2018, **76**, 359–367.

4 (*a*) U. H. F. Bunz, *Pure Appl. Chem.*, 2010, **82**, 953–968; (*b*) P.-Y. Gu, Z. Wang and Q. Zhang, *J. Mater. Chem. B*, 2016, **4**, 7060–7074.

5 S. S. Zade and M. Bendikov, *J. Phys. Org. Chem.*, 2012, **25**, 452–461.

6 (*a*) I. G. Stara and I. Stary, *Sci. Synth.*, 2010, **45b**, 885–953; (*b*) Y. Shen and C.-F. Chen, *Chem. Rev.*, 2011, **112**, 1463–1535; (*c*) C.-F. Chen and Y. Shen, *Helicene Chemistry From Synthesis to Applications*, Springer, Berlin, Heidelberg, 2017.

7 (*a*) N. Saleh, C. Shen and J. Crassous, *Chem. Sci.*, 2014, **5**, 3680–3694; (*b*) J. Bosson, J. Gouin and J. Lacour, *Chem. Soc. Rev.*, 2014, **43**, 2824–2840; (*c*) P. Aillard, A. Voituriez and A. Marinetti, *Dalton Trans.*, 2014, **43**, 15263–15278; (*d*) M. Gingras, *Chem. Soc. Rev.*, 2013, **42**, 1051–1095.

8 (*a*) M. Li, H.-Y. Lu, C. Zhang, L. Shi, Z. Tang and C.-F. Chen, *Chem. Commun.*, 2016, **52**, 9921–9924; (*b*) M. Li, Y. Niu, X. Zhu, Q. Peng, H.-Y. Lu, A. Xia and C.-F. Chen, *Chem. Commun.*, 2014, **50**, 2993–2995; (*c*) M. Li, W. Yao, J.-D. Chen, H.-Y. Lu, Y. Zhao and C.-F. Chen, *J. Mater. Chem. C*, 2014, **2**, 8373–8380.

9 (*a*) I. H. Delgado, S. Pascal, A. Wallabregue, R. Duwald, C. Besnard, L. Guenee, C. Nancoz, E. Vauthey, R. C. Tovar, J. L. Lunkley, G. Muller and J. Lacour, *Chem. Sci.*, 2016, **7**, 4685–4693; (*b*) J. Bosson, G. M. Labrador, S. Pascal, F.-A. Miannay, O. Yushchenko, H. Li, L. Bouffier, N. Sojic, R. C. Tovar, G. Muller, D. Jacquemin, A. D. Laurent, B. Le Guennic, E. Vauthey and J. Lacour, *Chem.–Eur. J.*, 2016, **22**, 18394–18403; (*c*) S. Pascal, C. Besnard, F. Zinna, L. Di Bari, B. Le Guennic, D. Jacquemin and J. Lacour, *Org. Biomol. Chem.*, 2016, **14**, 4590–4594.

10 H. Isla and J. Crassous, *C. R. Chim.*, 2016, **19**, 39–49.

11 E. M. Sánchez-Carnerero, A. R. Agarrabeitia, F. Moreno, B. L. Maroto, G. Muller, M. J. Ortiz and S. de la Moya, *Chem.–Eur. J.*, 2015, **21**, 13488–13500.

12 (*a*) K. Goto, R. Yamaguchi, S. Hiroto, H. Ueno, T. Kawai and H. Shinokubo, *Angew. Chem., Int. Ed.*, 2012, **51**, 10333–10336; (*b*) D. Sakamaki, D. Kumano, E. Yashima and S. Seki, *Angew. Chem., Int. Ed.*, 2015, **54**, 5404–5407; (*c*) X. Geng, J. P. Donahue, J. T. Mague and R. A. Pascal Jr, *Angew. Chem., Int. Ed.*, 2015, **54**, 13957–13960.

13 For a recent study describing terminal-end growth of helical skeletons up to [13]helicene frameworks, see S. K. Pedersen, K. Eriksen and M. Pittelkow, *Angew. Chem., Int. Ed.*, 2019, **58**(51), 18419–18423.

14 (*a*) B. W. Laursen and F. C. Krebs, *Angew. Chem., Int. Ed.*, 2000, **39**, 3432–3434; (*b*) C. Herse, D. Bas, F. C. Krebs, T. Bürgi, J. Weber, T. Wesolowski, B. W. Laursen and

J. Lacour, *Angew. Chem., Int. Ed.*, 2003, **42**, 3162–3166; (*c*) F. Torricelli, J. Bosson, C. Besnard, M. Chekini, T. Bürgi and J. Lacour, *Angew. Chem., Int. Ed.*, 2013, **52**, 1796–1800.

15 R. Duwald, S. Pascal, J. Bosson, S. Grass, C. Besnard, T. Bürgi and J. Lacour, *Chem.–Eur. J.*, 2017, **23**, 13596–13601.

16 P. E. Eaton, G. R. Carlson and J. T. Lee, *J. Org. Chem.*, 1973, **38**, 4071–4073.

17 P. Ruiz-Castillo and S. L. Buchwald, *Chem. Rev.*, 2016, **116**, 12564–12649.

18 S. H. Cho, J. Yoon and S. Chang, *J. Am. Chem. Soc.*, 2011, **133**, 5996–6005.

19 N. Gommermann, C. Koradin and P. Knochel, *Synthesis*, 2002, **2002**, 2143–2149.

20 For the formation of **K4**, the use of polyphosphoric acid (PPA) at 100 °C for 20 hours was preferred over Eaton's reagent.

21 H. Tanaka, M. Ikenosako, Y. Kato, M. Fujiki, Y. Inoue and T. Mori, *Commun. Chem.*, 2018, **1**, 38.

22 For a review on the influence of the twisting of polyacenes on their optical properties, see A. Bedi and O. Gidron, *Acc. Chem. Res.*, 2019, **52**, 2482–2490.

23 Strong ECD signals are observed in the UV domain for **1–3**, with $\Delta\varepsilon$ up to 107 M$^{-1}$ cm$^{-1}$ for **3** at 298 nm. It is also the case for **4–6**, with $\Delta\varepsilon$ up to 240 M$^{-1}$ cm$^{-1}$ for **6** at 286 nm.

24 (*a*) Y. Yamamoto, H. Sakai, J. Yuasa, Y. Araki, T. Wada, T. Sakanoue, T. Takenobu, T. Kawai and T. Hasobe, *Chem.–Eur. J.*, 2016, **22**, 4263–4273; (*b*) T. Biet, T. Cauchy, Q. Sun, J. Ding, A. Hauser, P. Oulevey, T. Burgi, D. Jacquemin, N. Vanthuyne, J. Crassous and N. Avarvari, *Chem. Commun.*, 2017, **53**, 9210–9213; (*c*) T. Otani, A. Tsuyuki, T. Iwachi, S. Someya, K. Tateno, H. Kawai, T. Saito, K. S. Kanyiva and T. Shibata, *Angew. Chem., Int. Ed.*, 2017, **56**, 3906–3910; (*d*) Z. Dominguez, R. Lopez-Rodriguez, E. Alvarez, S. Abbate, G. Longhi, U. Pischel and A. Ros, *Chem.–Eur. J.*, 2018, **24**, 12660–12668; (*e*) M. Satoh, Y. Shibata and K. Tanaka, *Chem.–Eur. J.*, 2018, **24**, 5434–5438; (*f*) H. Tanaka, Y. Kato, M. Fujiki, Y. Inoue and T. Mori, *J. Phys. Chem. A*, 2018, **122**, 7378–7384.

25 H. Tanaka, Y. Inoue and T. Mori, *ChemPhotoChem*, 2018, **2**, 386–402.

26 (*a*) T. Kaseyama, S. Furumi, X. Zhang, K. Tanaka and M. Takeuchi, *Angew. Chem., Int. Ed.*, 2011, **50**, 3684–3687; (*b*) T. Amako, K. Nakabayashi, A. Sudo, M. Fujiki and Y. Imai, *Org. Biomol. Chem.*, 2015, **13**, 2913–2917; (*c*) J. R. Brandt, X. Wang, Y. Yang, A. J. Campbell and M. J. Fuchter, *J. Am. Chem. Soc.*, 2016, **138**, 9743–9746; (*d*) M. Gon, R. Sawada, Y. Morisaki and Y. Chujo, *Macromolecules*, 2017, **50**, 1790–1802; (*e*) H. Nishimura, K. Tanaka, Y. Morisaki, Y. Chujo, A. Wakamiya and Y. Murata, *J. Org. Chem.*, 2017, **82**, 5242–5249; (*f*) K. Takaishi, T. Yamamoto, S. Hinoide and T. Ema, *Chem.–Eur. J.*, 2017, **23**, 9249–9252; (*g*) C. Maeda, K. Nagahata, K. Takaishi and T. Ema, *Chem. Commun.*, 2019, **55**, 3136–3139; (*h*) A. Taniguchi, D. Kaji, N. Hara, R. Murata, S. Akiyama, T. Harada, A. Sudo, H. Nishikawa and Y. Imai, *RSC Adv.*, 2019, **9**, 1976–1981.